Hollow Nanostructures

DOI: 10.1002/ange.201406484

Hierarchical Zn/Ni-MOF-2 Nanosheet-Assembled Hollow Nanocubes for Multicomponent Catalytic Reactions**

*Zhicheng Zhang, Yifeng Chen, Su He, Jingchao Zhang, Xiaobin Xu, Yong Yang, Farhat Nosheen, Faisal Saleem, Wei He, and Xun Wang**

Abstract: *Metal-organic frameworks (MOFs) are potentially useful molecular materials that can exhibit structure flexibilities induced by some external stimuli. Such structure transformations can furnish MOFs with improved properties. The shape-controlled growth of MOFs combined with crystal-structure transformation is rarely achieved. Herein, we demonstrate the synthesis of hierarchical Zn/Ni-MOF-2 nanosheet-assembled hollow nanocubes (NAHNs) by a facile surfactant-free solvothermal approach. The unique nanostructures undergo crystal-structure transformation from Zn/Ni-MOF-5 nanocubes to Zn/Ni-MOF-2 nanosheets, which is analogous to the dissolution and recrystallization of inorganic nanocrystals. The present synthetic strategy to fabricate isostructural MOFs with hierarchical, hollow, and bimetallic nanostructures is expected to expand the diversity and range of potential applications of MOFs.*

Hierarchical architectures constructed from nano-building blocks with specific dimensions have attracted extensive interest because of their intriguing properties and various potential applications.[1–4] Self-assembly of nano-building blocks into a three-dimensional (3D) architecture synergistically combines the advantages of nanostructures and microstructures, which are less-pronounced in 2D and 1D structures. To date, enormous developments have been achieved for the fabrication of hierarchical structures involving biominerals,[5] chalcogenides,[6,7] metal oxides,[8,9] and noble metals.[3,10] Comparatively, rare are reports on the design of hierarchical metal–organic framework nanomaterials (MOFs).

MOFs, which are a class of highly crystalline hybrid porous materials, have received considerable attention owing to their topological architectures and diverse potential uses in many fields.[11–14] Since MOFs are constructed through the principle of coordination chemistry,[11] some chemical and physical stimuli may induce different effects in the crystal structure and thus furnish MOFs with flexibilities, such as stretching, rotational, "breathing", scissoring, inter-layer/network shifting, and coordination-bond cleavage/formation.[15–17] In this regard, structural transformations of MOFs have been extensively investigated, involving guest removal, guest exchange, ligand exchange, and molecular rearrangement.[18–20] These processes have tremendously stimulated research on the relationship between the structure and function at the molecular level. Up to now, the structural transformations have been mainly accomplished in the case of single-crystal-to-single-crystal transformations.[15–20]

To further enhance the inherent properties and endow MOF materials with multifunctionality, it is important to achieve morphology and size control while maintaining the inorganic–organic backbone. Nevertheless, compared with rich synthetic chemistry of nanocrystals, the shape-controlled growth of MOFs has been overlooked. It is documented that hollow nanomaterials (such as metals[21] and metal oxides[22]) can exhibit excellent properties differing from their solid counterparts with the advantages of high surface to volume ratio, large void space, and cost reduction, and thus find a wide scope of utility. On the contrary, the rational fabrication of hierarchical 3D MOF hollow nanostructures has rarely been reported and thus deserves much more research efforts. Herein, we demonstrate that hierarchical Zn/Ni-MOF-2 NAHNs can be solvothermally prepared in high yields using 1,4-benzenedicarboxylic acid (H_2BDC) as organic linkers, zinc and nickel ions as metallic nodes, *N*,*N*-dimethylacetamide (DMAC)/ethanol as a mixed solvent. The unique nanostructures were produced through the structural transformation from Zn/Ni-MOF-5 nanocubes to Zn/Ni-MOF-2 nanosheets (Scheme 1), based on which we suggest that in situ synthesized nanocubes may act as an additional supporting template and the evolution process is analogous to the dissolution and recrystallization of inorganic nanocrystals. Impressively, by depositing Pd clusters onto Zn/Ni-MOF-2 NAHNs, MOF-immobilized Pd hybrid nanomaterials were successfully fabricated, which exhibit excellent catalytic properties towards CO-based multicomponent alkoxycarbonylation reactions.

The morphology, structure, and composition of as-prepared hierarchical Zn/Ni-MOF-2 NAHNs were investigated by various characterization techniques. The scanning electron microscopy (SEM) images (Figure 1a and Figure S1a in the Supporting Information) show that the product consists of well-defined cubic structures with an edge length of 400–600 nm. Careful observation by the high-magnification SEM image (Figure 1b) shows that the surfaces of these cubes are

[*] Z. C. Zhang, S. He, J. C. Zhang, X. B. Xu, Y. Yang, F. Nosheen, F. Saleem, Prof. X. Wang
Department of Chemistry, Tsinghua University
Beijing, 100084 (China)
E-mail: wangxun@mail.tsinghua.edu.cn
Y. F. Chen, Prof. W. He
Department of Pharmacology and Pharmaceutical Sciences, School of Medicine and School of Life Sciences Tsinghua University
Beijing, 100084 (China)

[**] This work was supported by NSFC (91127040, 21221062), CPSF (2013M540085), and the State Key Project of Fundamental Research for Nanoscience and Nanotechnology (2011CB932402).

Supporting information for this article is available on the WWW under http://dx.doi.org/10.1002/anie.201406484.

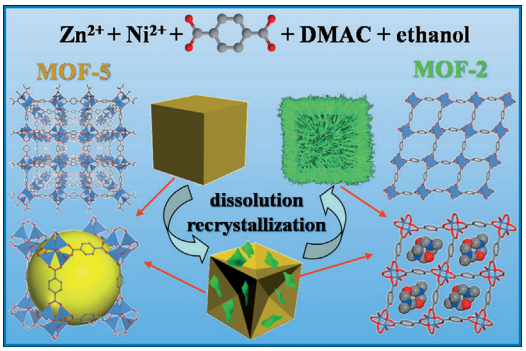

Scheme 1. Schematic illustration of crystal-structure transformation of a MOF combined with its shape evolution. Hydrogen atoms and terminal solvent molecules have been omitted for clarity. Yellow sphere indicates pore volume.

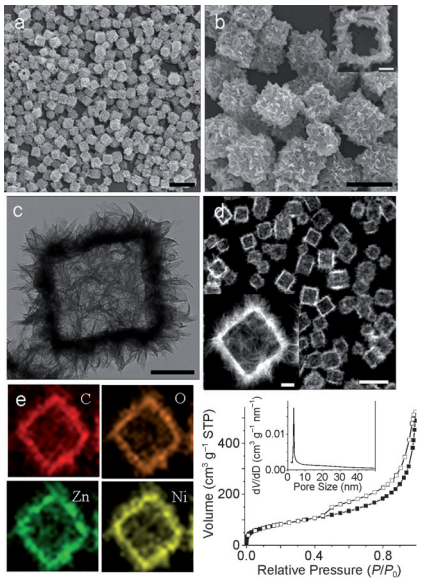

Figure 1. a,b) SEM (scale bars 2 μm and 1 μm, respectively), c) TEM (scale bar 200 nm), d) HAADF-STEM (scale bar 1 μm), e) EDX elemental mapping (of the inset in (d)) images, and f) nitrogen adsorption (■) and desorption (□) isotherms measured at 77 K of hierarchical Zn/Ni-MOF-2 NAHNs. Inset in (b): high-magnification SEM image, scale bar 200 nm, Inset in (d): HAADF-STEM image, scale bar 100 nm. Inset in (f): the corresponding pore size distribution.

highly rough and composed of numerous nanosheets. An individual broken nanocube was observed with an open gap and cavity (Figure 1b, inset), showing the hollow nature of these nanocubes. The transmission electron microscopy (TEM) (Figure 1c, Figure S1b) and high-angle annular dark-field scanning TEM (HAADF-STEM) (Figure 1d and Figure S1c) images further confirm the formation of hierarchical NAHNs, where the highly flexible nanosheets with an average thickness of sub-10 nm can be identified. Elemental mapping by energy-dispersive X-ray spectroscopy (EDX) shows that the elements C, O, Ni, and Zn are homogeneously distributed throughout the whole particle (Figure 1e). Fourier Transform Infrared (FT-IR) spectrum (Figure S2 in the Supporting Information) confirms the coordination interaction between metallic ions and carboxylic acid group of H_2BDC, as demonstrated by a red shift in the C=O stretching frequency to 1585 cm^{-1} from 1678 cm^{-1} for the uncoordinated building blocks H_2BDC.[23] The powder X-ray diffraction (PXRD) pattern (Figure S3) of the sample is similar to that reported for Cu or Zn MOF-2.[24,25] This result indicates that metal substitution in synthesis of mixed-metal MOFs can be achieved isostructurally to the homometallic counterparts. The chemical composition of hierarchical Zn/Ni-MOF-2 NAHNs was determined by inductively coupled plasma optical emission spectrometry (ICP-OES) and C, H, N elemental analysis, which confirms a chemical formula of $Ni_{5.9}Zn_{3.3}C_{32}H_{36}O_{22}N_{0.6}$. X-ray photoelectron (XPS) spectrum reveals that the samples are also composed of C, O, N, Ni, and Zn (Figure S4). The thermogravimetric (TG) curve (Figure S5) taken in air (nitrogen) exhibits significant weight loss in the temperature range of 300 °C to 420 °C (350 °C to 500 °C). A continuous weight loss below 300 °C (350 °C) can be attributed to the solvent liberation or the loss of guest molecules.[23] On the basis of the above results, it can be concluded that the sample is composed of Zn^{2+}, Ni^{2+}, BDC, and few guest molecules (DMAC and/or ethanol). The permanent porosity of hierarchical Zn/Ni-MOF-2 NAHNs was confirmed by nitrogen adsorption–desorption isotherms and pore size distribution measurements (Figure 1f). The sample adsorbs N_2 gas at 77 K, displaying a typical IV isotherms characteristic of mesoporous materials.[23,26] Furthermore, it was found that nitrogen uptake exhibits a notable increase at a low relative pressure ($P/P_0 < 0.01$), indicative of the inherent microporosity of the sample.[27] The pore size distribution derived from desorption data and calculated from BJH method (Figure 1f, inset) indicates that the sample exhibits a dominant pore diameter centered at 3.4 nm. BET specific surface area of the sample is 309 $m^2 g^{-1}$ (Langmuir surface area, 433 $m^2 g^{-1}$). The formation of mesoporosity in the hierarchical Zn/Ni-MOF-2 NAHNs may be ascribed to the voids resulting from the disorderly assembly of the flexible nanosheets.

To reveal the possible growth mechanism involved in the formation of hierarchical Zn/Ni-MOF-2 NAHNs, a series of control experiments were systematically conducted using the standard procedure. The reaction in the absence of the Ni precursor yielded Zn-MOF-5 cubic structures having diameters in the range of 100 nm–1 μm (Figure S6). While without the addition of the Zn precursor to the reaction solution, almost no solid matter appeared after the precipitation treatment, which may imply a preferential coordination interaction of the carboxylate group to Zn^{2+} over Ni^{2+}. In the synthesis, the use of mixed solvents with DMAC and ethanol is indispensable for the formation of hierarchical Zn/Ni-MOF-2 NAHNs. DMAC is used to dissolve the H_2BDC powder and serve as deprotonation of H_2BDC.[28] Different hollow nanostructures could be produced by the post treatment with ethanol. When the reaction time was shortened to 0.1 h, the product solution was centrifuged and then dispersed in DMAC, solid nanocubes could be obtained (Figure S7). But if the product was separated by centrifugation and then dispersed in a different volume of ethanol for a different time, three-dimensional mesoporous nanocubes (Figure 2a–c, Fig-

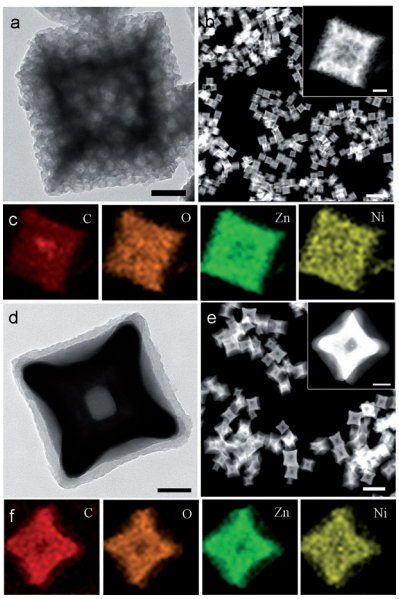

Figure 2. a) TEM (scale bar 100 nm), b) HAADF-STEM (scale bar 1 μm), and c) EDX mapping images of three-dimensional mesoporous nanocubes. d) TEM (scale bar 100 nm), e) HAADF-STEM (scale bar 500 nm), and f) EDX mapping images of concave nanocubes with hollow interior. Insets in (b) scale bar 100 nm and in (e) scale bar 100 nm show the corresponding high-magnification HAADF-STEM images.

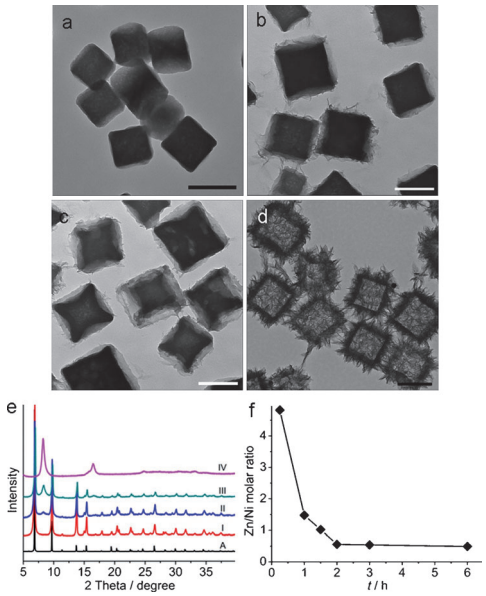

Figure 3. TEM (scale bars 500 nm) images of the products collected at different reaction time: a) 0.1 h, b) 1 h, c) 1.5 h, d) 2 h. e) XRD patterns of cubic crystalline MOF-5 (A) and the product collected at different reaction time: I) 0.1 h, II) 1 h, III) 1.5 h, IV) 2 h. f) Change in Zn/Ni molar ratio during 6 h based on EDX results.

ure S8), concave nanocubes with hollow interior (Figure 2 d–f, Figure S9), and nanocubes with a cavity (Figure S10) were produced. PXRD results revealed that these hollow nanostructures retained the MOF-5 crystalline lattice. The EDX results showed that the molar ratio of Zn to Ni was almost unchanged by post-treatment with ethanol. Additionally, with a reaction time of 3 h, porous nanocubes were formed when immersed in ethanol (Figure S11). Based on the above facts, we suggest that inner crystallites dissolve and migrate out to reduce the higher surface energies of the crystallite.[23] The increase in surface energy may be derived from the change of solvent polarity or kinetic control in the synthetic system.[23,29] The hollowing process deserves further study.

To gain further insight into the evolution process of hierarchical Zn/Ni-MOF-2 NAHNs, we monitored the solvothermal process by running the reactions under the same conditions but for different lengths of time (Figure 3). At reaction time of 0.1 h, the product consists of uniform cubic nanoparticles with a side length of 300–500 nm (Figure 3 a). Prolonging the reaction time to 1 h, the nanocubes have a darker contrast in the middle region than at the edges, indicating the formation of concave nanostructures, as also can be confirmed by SEM (Figure S12). Meanwhile, a small amount of flexible nanosheets were found to adhere to the outer surface of the concave nanocubes (Figure 3 b). As the reaction time was extended to 1.5 h, it was observed that the concave features became much more distinct and a large number of nanosheets appeared around the etched nanocubes (Figure 3 c). Perfect hierarchical NAHNs with a side length of 400–600 nm were ultimately produced and confirmed from TEM of samples at 2 h (Figure 3 d). Beyond 2 h, no significant change in either the size or structure was observed (Figure S13), suggesting that the reaction was complete. During the solvothermal process, the bulk crystal structure transformation from isoreticular MOF-5 to MOF-2 was confirmed by PXRD measurements (Figure 3 e). At 0.1 h, PXRD pattern of as-obtained nanocubes matches well with that of cubic crystalline Zn-MOF-5.[23,29] Then the mixed phase of MOF-5 and MOF-2 was observed at 1 h. With increasing the time to 1.5 h, the intensity of the diffraction peaks ascribed to MOF-2 increased relative to MOF-5. For the sample at 2 h, the peaks ascribed to MOF-5 vanished, leaving a single phase of MOF-2. On the basis of the above results, it may be speculated that original and etched nanocubes exhibit the MOF-5 crystal structure, while subsequently formed nanosheets have the MOF-2 crystal structure. Accordingly, by changing the reaction time, a crystal transformation occurs as shown by the gradual change in the PXRD pattern, which is consistent with corresponding TEM observations above. The time-domain composition change was revealed by EDX analysis (Figure 3 f, Figure S14), which shows that the molar ratio of Ni to Zn increased within 2 h and then reached equilibrium. In the initial stage, we suggest that Ni^{2+} partly substituted for Zn^{2+} in the frameworks which could retain the MOF-5 crystalline lattice,[30] indicative of the coordination flexibility of the polymeric architectures. Over time, the Zn/Ni-MOF-5 nanocubes were gradually etched, and the Zn/Ni-MOF-2 nanosheets were simultaneously formed and covered on the surface of the concave nanocubes, whose evolution processes are analogous to the dissolution and recrystallization of inorganic nanocrystals.[31] As a result of the continuous change of molar ratio of Zn to Ni until the reaction has proceed for 2 h, combined with the distinct connectivity differences in the MOF-5 and MOF-2 crystal structures, we

suggest that the structural transformation should involve the cleavage and regeneration of coordination bonds between metal ions (Zn^{2+}/Ni^{2+}) and carboxylic acid groups. It is well established that Zn^{2+} and Ni^{2+} ions can both exist in either octahedral or tetrahedral geometries; However, in the presence of weak-field ligands, such as carboxylate and solvent molecules, Zn^{2+} prefers tetrahedral coordination while Ni^{2+} favors octahedral coordination.[32] This is in good agreement with the coordination modes of metal ions in MOF-5 and MOF-2 crystal structures. FT-IR spectra of the samples obtained at different reaction times further confirmed the change in coordination of the carboxylate groups to metal ions, where the absorption peak attributed to the coordination of the carboxylic acid group to Zn^{2+} decreased in strength, accompanied with the increase in strength of the absorption peak ascribed to Ni^{2+} carboxylate bonds (Figure S15). Based on all the above results, we propose that the fast formation of Zn/Ni-MOF-5 nanocubes may result from the control of reaction kinetics, owing to the high concentration of metal ions and organic ligands in the initial stage. Then thermodynamically favored Zn/Ni-MOF-2 nanosheets are finally formed. During the shape evolution process, the pre-formed Ni/Zn-MOF-5 nanocubes could be considered as an additional supporting template, and then these isostructural MOF-5 nanocubes are structurally unstable in this synthetic system and are susceptible to flexible structural transformation into nanosheets with the MOF-2 crystal structure. The transformation probably originates from the destabilization of the building units, and/or different coordination numbers and geometries, caused by some external stimuli.

To demonstrate the structural advantage in catalysis, we prepared Zn/Ni-MOF-2 NAHNs immobilized Pd clusters. After depositing 2.1 nm Pd clusters (Figure S16) onto Zn/Ni-MOF-2 NAHNs, the morphology of Zn/Ni-MOF-2 NAHNs could be maintained, and Pd clusters were uniformly loaded on Zn/Ni-MOF-2 NAHNs (Figure 4), as confirmed by EDX results (Figure S18), TEM, high-resolution TEM (HRTEM), HAADF-STEM (Figure S17d–f), and EDX mapping images. A Pd catalyzed alkoxycarbonylation of aryl halides (Figure 5a) is a convergent and direct route for fine chemical synthesis.[33,34] Figure 5b shows the kinetic curves for the alkoxycarbonylation reactions of Pd clusters, hierarchical Zn/Ni-MOF-2 NAHNs, hierarchical Zn/Ni- MOF-2 NAHNs immobilized Pd clusters, TiO_2 immobilized Pd clusters (Figure S19), and commercial Pd black (Alfa Aesar). Within 12 h, hierarchical Zn/Ni-MOF-2 NAHNs were found to be inactive, and hierarchical Zn/Ni-MOF-2 NAHNs immobilized Pd clusters exhibited significantly higher activity than TiO_2 immobilized Pd clusters, Pd clusters and Pd black. The morphologies of hierarchical Zn/Ni-MOF-2 NAHNs immobilized Pd clusters were retained after the catalytic reaction, as revealed by TEM images (Figure S20). Furthermore, substrates with both electron-donating (**2b**, **2c**, **2d**) and -withdrawing (**2e**, **2f**) groups reacted smoothly to give the corresponding products (Figure 5c, Figure S21). We suggest that the enhanced catalytic activity of hierarchical Zn/Ni-MOF-2 NAHNs immobilized Pd clusters could be ascribed to the unique structure and gas adsorption property of hierarchical Zn/Ni-MOF-2 NAHNs. That's to say, CO storage in the hierarchical Zn/Ni-MOF-2 NAHNs (Figure S22) may accelerate the catalytic process of Pd clusters (Figure 5d).

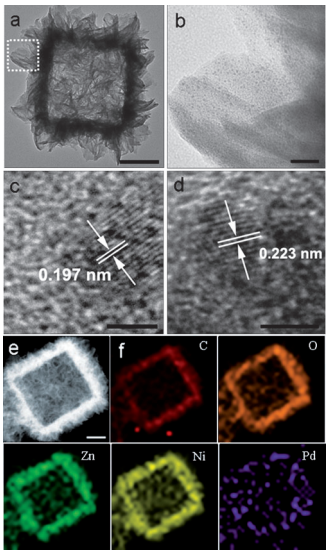

Figure 4. a,b) TEM (scale bars 200 nm and 20 nm, respectively), c,d) HRTEM (scale bar 2 nm), e) HAADF-STEM (scale bar 100 nm), and f) EDX mapping images of hierarchical Zn/Ni-MOF-2 NAHNs immobilized Pd clusters. b) is the magnified TEM image of the selected area marked by the white dashed line in (a).

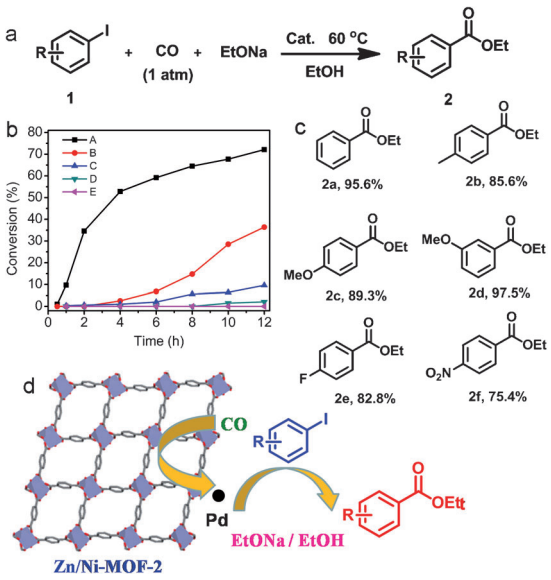

Figure 5. a) Alkoxycarbonylation reaction of aryl iodides. Reaction conditions: **1** (0.3 mmol), hierarchical Zn/Ni-MOF-2 NAHNs immobilized Pd clusters (0.008 equiv), EtONa (1.5 equiv) in ethanol at 60 °C, GC yields. b) Conversion (%) as a function of time in the alkoxycarbonylation reaction over hierarchical Zn/Ni-MOF-2 NAHNs immobilized Pd clusters (A), TiO_2 immobilized Pd clusters (B), Pd clusters (C), commercial Pd black (D), and hierarchical Zn/Ni-MOF-2 NAHNs (E). c) Products and yields of isolated products from the alkoxycarbonylation of aryl iodides catalyzed by hierarchical Zn/Ni-MOF-2 NAHNs immobilized Pd clusters for 24 h. d) Schematic representation of alkoxycarbonylation reaction of aryl iodides over hierarchical Zn/Ni-MOF-2 NAHNs immobilized Pd clusters.

In summary, we have successfully prepared hierarchical Zn/Ni-MOF-2 NAHNs by a facile solvothermal route without the assistance of any surfactants. The unique nanostructures undergo the crystal structure transformation from in situ synthesized Zn/Ni-MOF-5 nanocubes to Zn/Ni-MOF-2 nanosheets. During the shape evolution process, we suggest that the pre-formed nanocubes may function as an additional supporting template. We believe that such transformations will undoubtedly become an essential synthetic strategy in the design and synthesis of novel functional MOF hybrid nanomaterials, and bring more opportunities to the research and real application of MOFs.

Received: June 23, 2014
Published online: July 25, 2014

Keywords: aryl iodides · heterogeneous catalysis · hollow nanostructures · metal–organic frameworks · structure transformation

[1] K. Miszta, J. D. Graaf, G. Bertoni, D. Dorfs, R. Brescia, S. Marras, L. Ceseracciu, R. Cingolani, R. V. Roij, M. Dijkstra, L. Manna, *Nat. Mater.* **2011**, *10*, 872 – 876.
[2] A. Tao, P. Sinsermsuksakul, P. D. Yang, *Nat. Nanotechnol.* **2007**, *2*, 435 – 440.
[3] H. B. Yao, H. Y. Fang, X. H. Wang, S. H. Yu, *Chem. Soc. Rev.* **2011**, *40*, 3764 – 3785.
[4] L. Zhang, H. B. Wu, S. Madhavi, H. H. Hng, X. W. Lou, *J. Am. Chem. Soc.* **2012**, *134*, 17388 – 17391.
[5] F. Nudelman, N. A. J. M. Sommerdijk, *Angew. Chem.* **2012**, *124*, 6686 – 6700; *Angew. Chem. Int. Ed.* **2012**, *51*, 6582 – 6596.
[6] S. F. Zhuo, Y. Xu, W. W. Zhao, J. Zhang, B. Zhang, *Angew. Chem.* **2013**, *125*, 8764 – 8768; *Angew. Chem. Int. Ed.* **2013**, *52*, 8602 – 8606.
[7] Y. Q. Lei, S. Y. Song, W. Q. Fan, Y. Xing, H. J. Zhang, *J. Phys. Chem. C* **2009**, *113*, 1280 – 1285.
[8] J. S. Hu, L. S. Zhong, W. G. Song, L. J. Wan, *Adv. Mater.* **2008**, *20*, 2977 – 2982.
[9] D. F. Zhang, L. D. Sun, C. J. Jia, Z. G. Yan, L. P. You, C. H. Yan, *J. Am. Chem. Soc.* **2005**, *127*, 13492 – 13493.
[10] H. L. Gao, L. Xu, F. Long, Z. Pan, Y. X. Du, Y. Lu, J. Ge, S. H. Yu, *Angew. Chem.* **2014**, *126*, 4649 – 4654; *Angew. Chem. Int. Ed.* **2014**, *53*, 4561 – 4566.
[11] O. M. Yaghi, M. O. Keeffe, N. W. Ockwig, H. K. Chae, M. Eddaoudi, J. Kim, *Nature* **2003**, *423*, 705 – 714.
[12] G. Férey, *Chem. Soc. Rev.* **2008**, *37*, 191 – 214.
[13] T. Uemura, N. Yanai, S. Kitagawa, *Chem. Soc. Rev.* **2009**, *38*, 1228 – 1236.
[14] G. Lu, S. Z. Li, Z. Guo, O. K. Farha, B. G. Hauser, X. Y. Qi, Y. Wang, X. Wang, S. Y. Han, X. G. Liu, J. S. DuChene, H. Zhang, Q. C. Zhang, X. D. Chen, J. Ma, S. C. J. Loo, W. D. Wei, Y. H. Yang, J. T. Hupp, F. W. Huo, *Nat. Chem.* **2012**, *4*, 310 – 316.
[15] D. X. Xue, W. X. Zhang, W. M. Chen, H. Z. Wang, *Chem. Commun.* **2008**, 1551 – 1553.
[16] O. Ohmori, M. Kawano, M. Fujita, *J. Am. Chem. Soc.* **2004**, *126*, 16292 – 16293.
[17] E. Y. Lee, M. P. Suh, *Angew. Chem.* **2004**, *116*, 2858 – 2861; *Angew. Chem. Int. Ed.* **2004**, *43*, 2798 – 2801.
[18] J. P. Zhang, Y. Y. Lin, W. X. Zhang, X. M. Chen, *J. Am. Chem. Soc.* **2005**, *127*, 14162 – 14163.
[19] W. Kaneko, M. Ohba, S. Kitagawa, *J. Am. Chem. Soc.* **2007**, *129*, 13706 – 13712.
[20] N. Zhao, F. X. Sun, H. M. He, J. T. Jia, G. S. Zhu, *Cryst. Growth Des.* **2014**, *14*, 1738 – 1743.
[21] a) S. E. Skrabalak, J. Y. Chen, Y. G. Sun, X. M. Lu, L. Au, C. M. Cobley, Y. N. Xia, *Acc. Chem. Res.* **2008**, *41*, 1587 – 1595; b) Z. C. Zhang, Y. Yang, F. Nosheen, P. P. Wang, J. C. Zhang, J. Zhuang, X. Wang, *Small* **2013**, *9*, 3063 – 3069.
[22] a) L. Zhang, H. B. Wu, X. W. Lou, *J. Am. Chem. Soc.* **2013**, *135*, 10664 – 10672; b) Y. D. Yin, R. M. Rioux, C. K. Erdonmez, S. Hughes, G. A. Somojai, A. P. Alivisatos, *Science* **2004**, *304*, 711 – 714; c) J. S. Chen, Y. L. Tan, C. M. Li, Y. L. Cheah, D. Y. Luan, S. Madhavi, F. Y. C. Boey, L. A. Archer, X. W. Lou, *J. Am. Chem. Soc.* **2010**, *132*, 6124 – 6130.
[23] Z. C. Zhang, Y. F. Chen, X. B. Xu, J. C. Zhang, G. L. Xiang, W. He, X. Wang, *Angew. Chem.* **2014**, *126*, 439 – 443; *Angew. Chem. Int. Ed.* **2014**, *53*, 429 – 433.
[24] J. X. Liu, B. Lukose, O. Shekhah, H. K. Arslan, P. Weidler, H. Gliemann, S. Brase, S. Grosjean, A. Godt, X. L. Feng, K. Mullen, I. B. Magdau, T. Heine, C. Woll, *Sci. Rep.* **2012**, *2*, 921 – 925.
[25] H. L. Li, M. Eddaoudi, T. L. Groy, O. M. Yaghi, *J. Am. Chem. Soc.* **1998**, *120*, 8571 – 8572.
[26] D. P. Serrano, J. Aguado, J. M. Escola, J. M. Podriguez, A. Peral, *Chem. Mater.* **2006**, *18*, 2462 – 2464.
[27] Y. Y. Karabach, M. F. C. Guedes da Silva, M. N. Kopylovich, B. Gil-Hernandez, J. Sanchiz, A. M. Kirillov, A. J. L. Pombeiro, *Inorg. Chem.* **2010**, *49*, 11096 – 11105.
[28] O. Karagiaridi, W. Bury, J. E. Mondloch, J. T. Hupp, O. K. Farha, *Angew. Chem.* **2014**, *126*, 4618 – 4628; *Angew. Chem. Int. Ed.* **2014**, *53*, 4530 – 4540.
[29] L. C. He, Y. Liu, J. Z. Liu, Y. S. Xiong, J. Z. Zheng, Y. L. Liu, Z. Y. Tang, *Angew. Chem.* **2013**, *125*, 3829 – 3833; *Angew. Chem. Int. Ed.* **2013**, *52*, 3741 – 3745.
[30] C. K. Brozek, M. Dinca, *J. Am. Chem. Soc.* **2013**, *135*, 12886 – 12891.
[31] T. R. Zhang, J. P. Ge, Y. X. Hu, Q. Zhang, S. Aloni, Y. D. Yin, *Angew. Chem.* **2008**, *120*, 5890 – 5895; *Angew. Chem. Int. Ed.* **2008**, *47*, 5806 – 5811.
[32] S. R. Caskey, A. J. Matzger, *Inorg. Chem.* **2008**, *47*, 7942 – 7944.
[33] Y. H. Hu, J. Liu, Z. X. Lu, X. C. Luo, H. Zhang, Y. Lan, A. W. Lei, *J. Am. Chem. Soc.* **2010**, *132*, 3153 – 3158.
[34] J. H. Liu, J. Chen, C. G. Xia, *J. Catal.* **2008**, *253*, 50 – 56.

